Available online at www.sciencedirect.com
SCIENCE DIRECT®
International Journal of Mass Spectrometry 228 (2003) 439–456
International Journal of Mass Spectrometry
www.elsevier.com/locate/ijms

Structure, thermochemistry, and reactivity of MS_n^+ cations (M = V, Mo; n = 1–3) in the gas phase

Ilona Kretzschmar[a,*], Detlef Schröder[a], Helmut Schwarz[a], P.B. Armentrout[b,1]

[a] *Institut für Chemie der Technischen Universität Berlin, Straße des 17. Juni 135, D-10623 Berlin, Germany*
[b] *Department of Chemistry, University of Utah, Salt Lake City, UT 84112, USA*

Received 27 November 2002; accepted 18 March 2003

Dedicated to Helmut Schwarz on the occasion of his 60th birthday.

Abstract

The reactions of MS_n^+ (M = V, Mo; n = 0–2) with CS_2 and COS have been studied using guided-ion beam (GIB) or Fourier-transform ion-cyclotron resonance (FTICR) mass spectrometry. The GIB studies give insight into the thermochemistry of the polysulfide species, whereas FTICR reveals their reactivity and yields kinetic parameters. Density functional calculations complement the experimental results and highlight the effect of geometry and spin multiplicity on reactivity. The following binding energies (all in eV) are derived: $D_0(SV^+–S) = 3.89 \pm 0.11$, $D_0(V^+–S_2) = 3.25 \pm 0.14$, $D_0(S_2V^+–S) = 3.44 \pm 0.16$, $D_0(SV^+–S_2) = 2.97 \pm 0.19$, $D_0(V^+–CS_2) = 1.18 \pm 0.13$, $D_0(Mo^+–S) = 3.68 \pm 0.06$, $D_0(SMo^+–S) = 4.10 \pm 0.10$, $D_0(Mo^+–S_2) = 3.42 \pm 0.11$, $D_0(S_2Mo^+–S) = 3.37 \pm 0.09$, $D_0(SMo^+–S_2) = 3.11 \pm 0.13$, $D_0(Mo^+–CS) = 1.68 \pm 0.14$, and $D_0(Mo^+–CS_2) = 0.70 \pm 0.13$. An alternating trend is found for the MS_n^+ bond dissociation energies (n = 1–3), which is rationalized by a combination of electronic and geometrical effects.

Keywords: GIB; FTICR; Mass spectrometry; Metal sulfide cation; Thermochemistry

1. Introduction

Metal polysulfides are important in many areas ranging from catalysis to biology and material science [1–3]. The recognition of their importance in biology came with the discovery of non-heme iron containing metal units in succinate dehydrogenase and DPNH dehydrogenase [4]. Further research soon revealed that these units are comprised of iron–sulfur clusters such as Fe_2S_2, Fe_3S_4, and Fe_4S_4. Although thought to be important "only" in electron transfer processes, we know today that they are also involved in many other functions such as substrate binding, catalysis, regulation, and sensing [5–8]. Interestingly, not only iron sulfides, but also vanadium and molybdenum have been found in certain metal enzyme cores important for the biological nitrogen cycle [9]. Nitrogen fixation as the key step occurs as the reduction of N_2 to NH_4^+ catalyzed by nitrogenase enzymes. The active site of these enzymes is a complicated MFe_7S_9 [10] cluster with cubic MFe_3S_4 units in which M can be either iron, vanadium, or molybdenum (Scheme 1).

* Corresponding author. Present address: Electrical Engineering, Yale University, 15 Prospect St., New Haven, CT 06520, USA. Tel.: +1-20-343-24-088; fax: +1-20-343-26-420.
E-mail addresses: ilona.kretzschmar@yale.edu (I. Kretzschmar), armentrout@chem.utah.edu (P.B. Armentrout).
[1] Co-corresponding author.

1387-3806/$ – see front matter
doi:10.1016/S1387-3806(03)00137-4

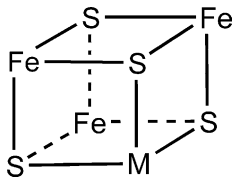

Scheme 1.

Further, it is believed that the so-called P cluster consisting of two Fe_4S_4 cubes with a common S corner and a second Fe_4S_4 cluster regulate electron transfer through the enzyme [11]. In such cubane-like entities, each metal atom bears three sulfur ligands in its coordination sphere. Conceptually, the M_4S_4 cluster can be split into 4MS, $2M_2S_2$, MS_2/2MS/M, or MS_3/MS/2M subunits. Understanding of the cubic M_4S_4 may thus be improved by consideration of the bonding situations in these fragments [12].

Here, we report on the thermochemistry, reactivity, and structure of mononuclear transition-metal polysulfide cations MS_n^+ (M = V, Mo; n = 1–3). The emphasis lies on the structural dichotomy of the metal polysulfide cations—the sulfur ligand enables formation of structures containing persulfo, di- and trisulfur as well as single sulfur ligands. Comparison with earlier results on the polysulfide cations of iron [13] reveals differences as well as similarities of V, Fe, and Mo in the coordination sphere of sulfur.

2. Methods

Most experiments were performed with a guided-ion beam (GIB) mass spectrometer, which has been described previously [14,15]. Briefly, M^+ (M = V, Mo) ions are formed in a dc discharge flow tube (DC/FT) source, in which energetic Ar^+ ions sputter M^+ ions from a negatively charged (−1.5 to −2 kV) cathode made of the metal to be studied. The ions formed in the source are then swept through a meter-long flow tube containing a 10% argon in helium buffer gas, at a total pressure of 0.9–1.3 mbar. The ions undergo ~10^5 collisions with the buffer gas as they traverse the flow tube, which helps to cool the ions to room temperature. However, it has been shown that helium is not always effective at quenching the excited electronic states of transition-metal ions [16–18]. Therefore, small amounts (0.013 mbar or less) of methane cooling gas are added to the flow tube in the case of bare metal cation beams to facilitate additional cooling of the metal cations. MS_n^+ (n = 1, 2) are generated by addition of a small amount of carbonyl sulfide (COS) to the flow tube.

Ions produced in the source are accelerated and passed through a magnetic sector for mass selection. The mass-selected ion beam is then focused into the entrance of a radio frequency (rf) octopole ion guide [19], whose dc potential with respect to the ion source determines the kinetic energy of the ion beam. The rf potential on the octopole rods radially confines the ions and guides them through a gas cell, where a neutral reactant is introduced at pressures low enough ($<10^{-4}$ mbar) to ensure single collision conditions. This was demonstrated by explicit pressure dependence measurements for the reaction of Mo^+ with CS_2. In all other systems, the probability of secondary collisions is less than 1% even for the largest cross-sections measured here. Both product and unreacted primary ions are extracted from the octopole and passed through a quadrupole mass filter for mass analysis. Finally, ions are detected with a secondary-electron scintillation ion detector and counted using standard pulse-counting techniques. This process is repeated at different collision energies simply by adjusting the dc potential of the octopole with respect to the ion source. Conversion of the raw ion intensities into cross-sections and the calibration of the absolute energy scale are treated as described previously [14]. The accuracy of the product cross-section magnitudes is estimated to be ±20%, and the uncertainty in the absolute energy scale is ±0.05 eV (lab). Laboratory energies are converted to energies in the center-of-mass frame using $E_{CM} = E_{lab} \times M/(M + m)$, where M and m are the masses of the neutral and ionic reactants, respectively.

$$\sigma(E) = \sigma_0 \sum g_i \frac{(E + E_i - E_0)^n}{E} \quad (1)$$

Energy thresholds for product formation at 0 K, E_0, are obtained by modeling the cross-sections using Eq. (1), where σ_0 is an energy-independent scaling factor, and E is the relative kinetic energy. E_0 and n are treated as adjustable fitting parameters. The summation is over the rovibrational states of the reactants having energies E_i and populations g_i ($\sum g_i = 1$). Before comparison to the data, Eq. (1) is convoluted over the kinetic energy distributions of both reactants. Because the convoluted form of Eq. (1) explicitly accounts for all of the energy available to the reaction, the optimized value of E_0 is interpreted as the threshold energy at 0 K. Uncertainties in the values of E_0 obtained using Eq. (1) represent one standard deviation (if not stated otherwise) and are derived from the range of fitting parameters that yield acceptable fits coupled with the uncertainties in the absolute energy scale. Vibrational frequencies used to account for rovibrational energies are: $\nu(VS^+) = 531.9\,cm^{-1}$; $\nu(VS_2{}^+) = 235.1, 611.5, 634.0\,cm^{-1}$; $\nu(MoS^+) = 529.3\,cm^{-1}$; $\nu(MoS_2^+) = 200.2, 528.7$, and $538.7\,cm^{-1}$ as obtained from density functional calculations.

A few additional experiments use a Spectrospin CMS 47X Fourier-transform ion-cyclotron resonance (FTICR) mass spectrometer equipped with an external ion source as described elsewhere [20,21]. In brief, M^+ is generated by laser ablation of a metal target, the ions are transferred via a series of potentials and ion lenses to the ICR cell in which they are stored in the field of a 7.05 T superconducting magnet. Mass-selected $^{51}V^+$ and $^{97}Mo^+$ are then thermalized by unreactive collisions with pulsed-in argon buffer gas, followed by re-isolation of the metal ion and monitoring the reaction with COS leaked-in at pressures of about 10^{-8} mbar. The experimental second-order rate constants are evaluated assuming the pseudo-first-order kinetic approximation after calibration of the measured pressures and acknowledgment of the ion gauge sensitivities. The rate constants of consecutive reactions are determined by numerical kinetic modeling [22]. The error of the absolute rate constants is ±30%, and the ion temperature is assumed as 298 K [23].

In the complementary theoretical investigations, the geometries of the polysulfides are obtained using the B3LYP hybrid functional [24] implemented in Gaussian 94 [25]. The B3LYP functional has been found to produce reasonable geometries for transition-metal complexes, although care needs to be taken in some systems where electron correlation dominates [26]. For species containing metals of the first transition row, the Wachters-Hay all-electron basis sets are combined with the scaling factors of Raghavachari and Trucks [27], and the standard all-electron 6-311+G(2d,p) basis set implemented in Gaussian 94 is employed for sulfur. For species containing molybdenum, the standard all-electron 3-21G basis sets are employed for molybdenum and sulfur. All minima and transition structures are characterized by frequency calculations with the exception of ^{1}TS obtained by a single-point calculation using the triplet geometry in the $VS_2{}^+$ system.

3. Experimental results

Prior to this study on the metal-polysulfide ions, considerable work has been done on the diatomic MS^+ ions (M = V, Fe, Mo). Thus, a careful investigation of the VS^+ cation led to a bond dissociation energy of $D_0(V^+–S) = 3.72 \pm 0.09$ eV [28,29] and a lower limit of 3.140 ± 0.005 eV for $D_0(SV^+–S)$ [28]. Accurate binding energies of $D_0(Fe^+–S) = 3.08 \pm 0.04$ eV, $D_0(SFe^+–S) = 3.59 \pm 0.12$ eV, and $D_0(Fe^+–S_2) = 2.31 \pm 0.31$ eV were derived from GIB measurements [13]. Further, a value of $D_{298}(S_2Fe^+–S) = 2.69 \pm 0.39$ eV was determined from the photodissociation (PD) threshold of $FeS_3{}^+$ [30]. Finally, an earlier study of $MoS_n{}^+$ ions using the FTICR bracketing technique and sequential S-transfer reactions of Mo^+ with COS and CS_2 led to $D_0(Mo^+–S) = D_0(SMo^+–S) = 3.82 \pm 0.61$ eV and $D_0(S_2Mo^+–S) = 4.34 \pm 0.61$ eV [31]. These values (although the molybdenum thermochemistry is superceded by present results) and auxiliary thermochemistry are compiled in Table 1.

Here, we concentrate our efforts on the mononuclear polysulfide cations $MS_n{}^+$ for M = V and Mo with

Table 1
Bond dissociation energies at 0 K

Species	D_0 (eV)	Species	D_0 (eV)	Species	D_0 (eV)
CO	11.109 (0.005)[a]	CS	7.37 (0.04)[b]	S_2	4.364 (0.005)
SC–O	6.88 (0.04)[c]	OC–S	3.140 (0.005)[c]	S_3	2.71 (0.08)
		CS_2	4.50 (0.04)[b,c]		
VS^+	3.72 (0.09)[d]	FeS^+	3.08 (0.04)[e]	MoS^+	3.68 (0.06)[f]
SV^+–S	3.89 (0.11)[f,g]	SFe^+–S	3.59 (0.12)[e]	SMo^+–S	4.10 (0.10)[f,g]
V^+–S_2	3.25 (0.14)[f,g]	Fe^+–S_2	2.31 (0.31)[e]	Mo^+–S_2	3.42 (0.11)[f,g]
S_2V^+–S	3.44 (0.16)[f]	S_2Fe^+–S	2.68 (0.39)[h]	S_2Mo^+–S	3.37 (0.09)[f]
SV^+–S_2	2.97 (0.19)[f]	SFe^+–S_2	2.11 (0.22)[h]	SMo^+–S_2	3.11 (0.13)[f]
V^+–CS	1.70 (0.08)[d]	Fe^+–CS	2.40 (0.12)[e]	Mo^+–CS	1.68 (0.14)[f]
V^+–CS_2	1.18 (0.13)[f]	Fe^+–CS_2	1.46 (0.11)[i]	Mo^+–CS_2	0.70 (0.13)[f]

[a] [42].
[b] [43].
[c] [44]. Corrected to 0 K using $H^\circ - H^\circ$ (298.15) values taken from the reference in footnote a.
[d] [28] and [29].
[e] [13].
[f] This work.
[g] Uncertainty is two standard deviations of the mean of multiple determinations, see text.
[h] Values taken from [30] and converted to 0 K using the enthalpy correction of 0.01 eV obtained from frequency calculations at the B3LYP/6-311+G* level.
[i] [45].

$n = 2, 3$ in order to compare their properties with the corresponding FeS_n^+ species. The pursued strategy is the investigation of sulfur-transfer processes according to reaction (2) with X = O and S, that is COS and carbon disulfide, respectively, as neutral reagents.

$$MS_n^+ + SCX \rightarrow MS_{n+1}^+ + CX \quad (2)$$

In the GIB experiment conducted at variable collision energies, several other reactions are observed in competition with sulfur transfer according to reaction (2). These side reactions are mentioned only if they appear to have direct relevance for the conclusions concerning the MS_n^+ species. Further, the GIB experiments are performed with CS_2 for which reaction (2) is generally endothermic whereas the complementary FTICR studies deal with the exothermic sulfur transfers occurring with COS.

3.1. GIB studies of VS_n^+

Upon reaction of mass-selected VS^+ with CS_2 at variable collision energies, VS_2^+, VCS_2^+, VCS^+, and V^+ are formed as ionic products according to reactions (3)–(6).

$$VS^+ + CS_2 \rightarrow VS_2^+ + CS \quad (3)$$

$$VS^+ + CS_2 \rightarrow VCS_2^+ + S \quad (4)$$

$$VS^+ + CS_2 \rightarrow VCS^+ + S_2 \quad (5)$$

$$VS^+ + CS_2 \rightarrow V^+ + [CS_3] \quad (6)$$

Formation of VS_2^+ according to reaction (3) is the least endothermic process and dominates the product spectrum below 5 eV (Fig. 1). The energy behavior of this channel is surprisingly complex. From an apparent threshold of about 0.25 eV, the cross-section of VS_2^+ rises steeply until about $E_{CM} = 1$ eV, where it rises more gradually, showing a change in slope at about 2 eV, and finally decreases above $E_{CM} = 4$ eV. The initial rise is straightforwardly assigned to reaction (3) and the decrease at high collision energies can be attributed to the competing V^+ channel. The intermediate behavior, however, points to contribution of at least one other process to the VS_2^+ cross-section. As far as the other products are concerned, these can be explained as follows. Formation of VCS_2^+ has an apparent threshold of 2.9 eV. The product can either correspond to a V^+–CS_2 complex with an intact CS_2

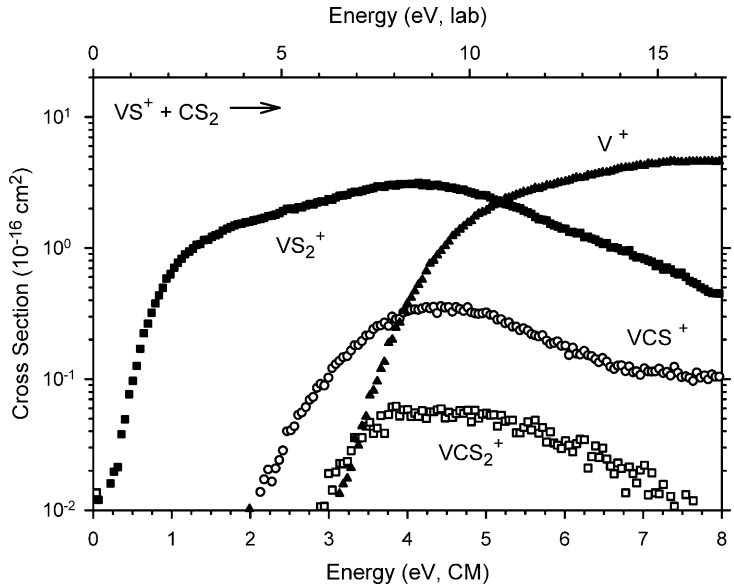

Fig. 1. Product cross-sections for the reactions of VS^+ with CS_2 to form VS_2^+ (■), VCS^+ (○), VCS_2^+ (□), and V^+ (▲) as a function of center-of-mass energy (lower axis) and laboratory energy (upper axis).

ligand or, after sulfur transfer, to a thiocarbonyl complex of SV^+–CS connectivity. Because previous calculations at the B3LYP/6-311+G* level of theory predict very similar stabilities of both isomers (V^+–CS_2 is 0.09 eV more stable [29]), no isomer distinction can be derived from the experimental VCS_2^+ cross-section. The threshold near 2 eV for the formation of VCS^+ in reaction (5) can only be rationalized if an S_2 molecule is formed as the neutral counterpart (Table 1). The product channel with the highest threshold is formation of V^+, reaction (6), which starts near 3.2 eV.

For more detailed considerations, the experimental cross-sections are analyzed with Eq. (1). Using the thresholds for reactions (3)–(5) given in Table 2, we arrive at $D_0(SV^+–S) = 3.97 \pm 0.10$ eV, $D_0(V^+–CS_2) = 1.12 \pm 0.18$ eV, and $D_0(V^+–CS) = 1.72 \pm 0.18$ eV. The latter value is in good agreement with a V^+–CS bond energy derived previously of 1.70 ± 0.08 eV [28,29]. A bond energy for the loss of an intact S_2-ligand of $D_0(V^+–S_2) = 3.33 \pm 0.13$ eV is derived from combining $D_0(SV^+–S) = 3.97 \pm 0.10$ eV, $D_0(V^+–S) = 3.72 \pm 0.09$ eV, and $D_0(S–S) = 4.364 \pm 0.005$ eV. The SV^+–S and V^+–S_2 binding energies are in good agreement with the exothermic formation of VS_2^+ observed in the $VS^+ + COS$ reaction and the very small and endothermic VS_2^+ cross-section ($\sigma_{max} < 0.02 \times 10^{-16}$ cm^2) observed for the $V^+ + CS_2$ reaction, respectively [28].

Some ambiguity is connected with the neutral(s) formed concomitantly with V^+, reaction (6), because the net formula [CS_3] can either stand for S and CS_2, S_2 and CS, or genuine CS_3 [32]. According to theory, the cyclic CS_3 molecule (thiodithiiranone) is 0.46 eV more stable than the CS_2/S couple [33], and experimental data indicate that CS_2/S is in turn 0.14 ± 0.04 eV more stable than S_2/CS (Table 1). The threshold measured for this process (Table 2) is consistent with either of the latter two channels, which can start at 3.72 ± 0.09 eV and 3.86 ± 0.10 eV, respectively. The observation that the VS_2^+ product decreases sharply as the V^+ cross-section rises demonstrates that the S_2/CS channel is a strong contributor to the production of V^+. Assuming that the latter is the only route to reaction (6), then the difference in the thresholds measured for reactions (3) and (6) leads to a direct

Table 2
Summary of parameters in Eq. (1) used for the fits of the cross-sections for the reactions of CS_2 and Xe with VS^+ and VS_2^+, respectively, reactions (3)–(12)

Reactants	Products	E_0 (eV)[a]	σ_0	n
$VS^+ + CS_2$	$VS_2^+ + CS$	0.53 (0.09)	1.66 (0.10)	1.7 (0.2)
	$VCS_2^+ + S$	2.60 (0.16)	0.12 (0.02)	1.5 (0.2)
	$VCS^+ + S_2$	2.14 (0.15)	0.35 (0.07)	1.9 (0.2)
	$V^+ + [CS_3]$	3.81 (0.14)	7.61 (0.82)	1.4 (0.1)
$VS_2^+ + Xe$	$VS^+ + S$	3.95 (0.23)	3.60 (0.88)	1.6 (0.3)
	$V^+ + S_2$	3.13 (0.06)	11.4 (2.5)	1.4 (0.2)
$VS_2^+ + CS_2$	$VS_3^+ + CS$	1.06 (0.15)	0.36 (0.07)	2.1 (0.2)
	$VCS_2^+ + S_2$	1.88 (0.13)	0.29 (0.05)	2.0 (0.2)
	$VS^+ + [CS_3]$	3.56 (0.16)	2.24 (0.46)	1.8 (0.2)
	$V^+ + [CS_4]$	3.13 (0.14)	2.12 (0.37)	1.8 (0.2)

[a] The E_0 values are the average of several threshold fits with uncertainties of one standard deviation.

determination of $D_0(V^+–S_2) = 3.28 \pm 0.17$ eV, in agreement with the value derived from an alternate route above.

$$VS_2^+ + Xe \rightarrow V^+ + S_2 + Xe \quad (7)$$

$$VS_2^+ + Xe \rightarrow VS^+ + S + Xe \quad (8)$$

The derived thermochemistry of gaseous VS_2^+ can be tested by CID with xenon (data not shown). The two ionic products V^+ and VS^+ observed are assigned to the dissociation reactions (7) and (8). Note that the absence of oxygen containing fragments, e.g., VO^+ and VSO^+, excludes interference by VO_2S^+ (data not shown). Reaction (7) has the lower threshold and reaches a cross-section of about 5.2 Å^2 near 7 eV, at which point it declines, apparently because of strong competition with reaction (8), which reaches a maximum magnitude of about 6.0 Å^2 near 12 eV. A small feature in the V^+ cross-section at high energies can be attributed to sequential losses of sulfur atoms. Because competition with the VS^+ channel affects the shape of the cross-section for V^+, the threshold for reaction (7) is obtained from an analysis of the total cross-section. Use of the total cross-section for analysis allows the cross-section to be reproduced over a much broader range of energies, thereby determining the n value in Eq. (1) more accurately. In dealing with small, strongly bound ions, energy transfer can be inefficient, in which case threshold CID is viewed most conservatively as yielding upper limits to the intrinsic dissociation energy [34]. However, the thresholds $E_0(V^+) = 3.13 \pm 0.06$ eV and $E_0(VS^+) = 3.95 \pm 0.23$ eV (Table 2) are in reasonable agreement with the values derived from analysis of reaction (3), $D_0(V^+–S_2) = 3.33 \pm 0.13$ eV and $D_0(VS^+–S) = 3.97 \pm 0.10$ eV, suggesting that both systems are providing good thermodynamic values.

When VS_2^+ ions are reacted with CS_2 in the GIB apparatus, four ionic products, VS_3^+, VCS_2^+, VS^+, and V^+, are observed according to reactions (9)–(12). Electron transfer to produce CS_2^+ is also observed as a minor product channel, but the cross-section is too noisy for analysis (data not shown).

$$VS_2^+ + CS_2 \rightarrow VS_3^+ + CS \quad (9)$$

$$VS_2^+ + CS_2 \rightarrow VCS_2^+ + S_2 \quad (10)$$

$$VS_2^+ + CS_2 \rightarrow VS^+ + [CS_3] \quad (11)$$

$$VS_2^+ + CS_2 \rightarrow V^+ + [CS_4] \quad (12)$$

The formation of VS_3^+ according to (9) parallels reaction (3) and is the least endothermic process with an apparent threshold of ca. 0.8 eV (Fig. 2). Next is reaction (10) beginning at about 1.5 eV, which can be rationalized as a ligand-exchange process in which CS_2 replaces a disulfur unit in the VS_2^+ cation; accordingly, the product should correspond to a $V(CS_2)^+$ complex with an intact CS_2 ligand. For the two high-energy

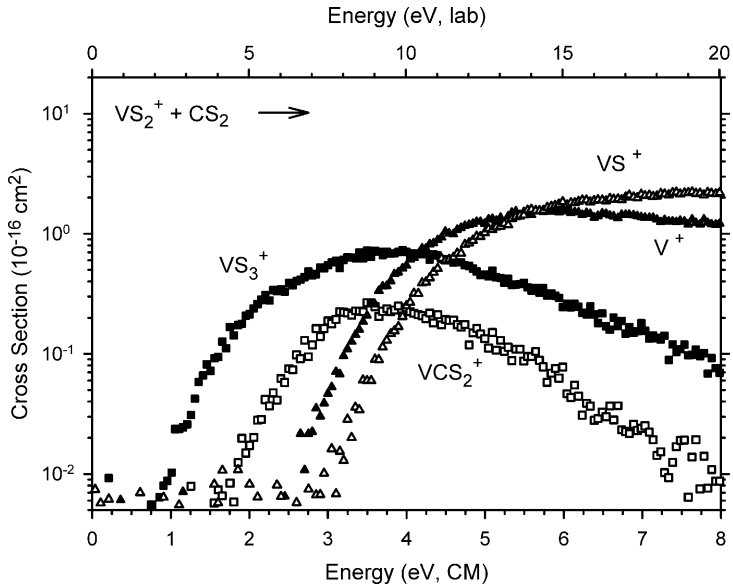

Fig. 2. Product cross-sections for the reactions of VS_2^+ with CS_2 to form VS_3^+ (■), VCS_2^+ (□), VS^+ (△), and V^+ (▲) as a function of center-of-mass energy (lower axis) and laboratory energy (upper axis).

products, V^+ and VS^+, again some difficulties are encountered as far as the straightforward assignment of the corresponding neutral counterparts is concerned.

Fitting of the VS_3^+ cross-section yields the parameters given in Table 2, which result in $D_0(VS_2^+–S) = 3.44 \pm 0.16$ eV. Likewise, the thresholds of reactions (10) and (12) can be combined to yield $D_0(V^+–CS_2) = 1.25 \pm 0.19$ eV, in good agreement with $D_0(V^+–CS_2) = 1.12 \pm 0.18$ eV derived from the threshold of reaction (4). Both values agree within their uncertainties and therefore are averaged to give $D_0(V^+–CS_2) = 1.18 \pm 0.13$ eV. Note that both VCS_2^+ cross-sections (Figs. 1 and 2) are relatively small and probably suffer from competition with the more pronounced product channels leading to the slightly larger uncertainty. As far as reactions (11) and (12) are concerned, the crucial question is the nature of the neutral species accompanying the ionic products. Direct comparison with the threshold for reaction (8) obtained upon CID of VS_2^+ with Xe reveals that the VS^+ threshold of reaction (11) is considerably lower. This finding suggests the formation of thiodithiiranone rather than $CS_2 + S$ or $CS + S_2$ in reaction (11). Given this assumption, the threshold measured suggests that $D_0(VS^+–S) = 4.02 \pm 0.16$ eV, in good agreement with values obtained from reactions (3) and (8). Further, the threshold for V^+ formation in reaction (12) is in good agreement with that of reaction (7); hence, there is no need to speculate about possible CS_4 isomers in reaction (12). Here, the threshold measured for $V^+ + S_2 + CS_2$ yields $D_0(V^+–S_2) = 3.13 \pm 0.14$ eV. Note that the sum of the V^+ and VS^+ cross-sections are not modeled in this system, because most of the VS^+ comes from decomposition of VS_3^+ rather than by direct CID; hence the competition between V^+ and VS^+ formation differs from that in the Xe system.

Threshold results for reactions (3), (8), and (11) provide values for $D_0(VS^+–S)$ of 3.97 ± 0.10 eV, 3.95 ± 0.23 eV, and 4.02 ± 0.16 eV, respectively, where the threshold for reaction (11) has been analyzed with the assumption of intact CS_3 being formed as the neutral product. The thresholds for reactions (6), (7), and (12) yield values for $D_0(V^+–S_2)$ of 3.28 ± 0.17 eV, 3.13 ± 0.06 eV, and 3.13 ± 0.14 eV, respectively, which can be combined with $D_0(V^+–S) = 3.72 \pm 0.09$ eV and $D_0(S–S) = 4.364 \pm 0.005$ eV to give values for $D_0(VS^+–S)$ of 3.92 ± 0.19 eV, 3.77 ± 0.11 eV,

and 3.77 ± 0.17 eV, respectively. Each of these values for $D_0(VS^+–S)$ is derived from a separately measured threshold, such that an average value for $D_0(VS^+–S)$ can be derived as 3.89 ± 0.11 eV, and a corresponding value for $D_0(V^+–S_2)$ of 3.25 ± 0.14 eV. These are weighted averages of all six results with an uncertainty of two standard deviations of the mean. Given this value for $D_0(SV^+–S)$, we can also combine our measurement of $D_0(S_2V^+–S) = 3.44 \pm 0.16$ eV with $D_0(S–S) = 4.364 \pm 0.005$ eV to obtain $D_0(SV^+–S_2) = 2.97 \pm 0.19$ eV.

3.2. FTICR studies of VS_n^+

Consistent with the GIB results, thermalized V^+ cations do not show significant reactivity towards CS_2 under FTICR conditions. This is a mere consequence of the thermochemistry of the putative sulfur-transfer reactions which are endothermic for vanadium because $D_0(S_nV^+–S) \ll D_0(SC–S) = 4.50 \pm 0.04$ eV for $n = 0$–2. For COS, however, consecutive sulfur transfer up to VS_4^+ is observed (reactions 13–16). These observations suggest a lower limit of $D_0(S_nV^+–S) = D_0(OC–S) = 3.140 \pm 0.005$ eV for $n = 0$–3. For VS^+, VS_2^+, and VS_3^+ formation in reactions (13)–(15), this lower limit agrees nicely with the bond energies derived above (Table 1).

$$V^+ + COS \rightarrow VS^+ + CO \quad (13)$$

$$VS^+ + COS \rightarrow VS_2^+ + CO \quad (14)$$

$$VS_2^+ + COS \rightarrow VS_3^+ + CO \quad (15)$$

$$VS_3^+ + COS \rightarrow VS_4^+ + CO \quad (16)$$

Provided appropriate thermalization of the V^+ cations, reaction (13) follows strict first-order behavior and yields a rate constant of $k_{(13)} = (3.4 \pm 1.0) \times 10^{-10}$ cm^3 s^{-1} molecule^{-1} [28]. Comparison with the collision rate constant of about 1×10^{-9} cm^3 molecule^{-1} s^{-1} indicates that sulfur transfer from COS to V^+ is only 34% efficient. Kinetic modeling of the intensity profiles of the VS_n^+ cations can be used to derive the rate constants of the consecutive sulfur-transfer processes. However, it turns out that single sets of exponential functions cannot reproduce the kinetic data of VS^+ and VS_2^+: either their formation is underestimated or the decay occurs too slowly. Such behavior can be expected if consecutive reactions with considerable exothermicities are examined in FTICR, where the overall pressures are rather low (typically 10^{-9} to 10^{-7} mbar) [35]. Specifically, the GIB results imply that reactions (13) and (14) are exothermic by 0.58 ± 0.09 eV and 0.75 ± 0.11 eV, respectively. Under FTICR conditions, collisional cooling is slow such that part of this exothermicity remains in the products and thereby decreases the exothermic reactivity of these product ions towards COS. Furthermore, the $V(S_2)^+/SVS^+$ isomerism could also play a role in the case of VS_2^+; however, quenching of excess internal energy and isomerism cannot be distinguished with the kinetic data available. With appropriate inclusion of this phenomenon in the kinetic modeling [35], the relative rates for the formations of VS_n^+ according to reactions (13)–(16) behave as 6:6:3:1.

3.3. GIB studies of MoS_n^+

The consecutive reactions of Mo^+ with COS under FTICR conditions lead to stepwise S-atom transfer up to MoS_5^+ [31]. The two main ionic products when Mo^+ is reacted with CS_2 in the GIB apparatus are MoS^+ and $MoCS^+$ (Fig. 3). Minor products observed are MoC^+ and CS_2^+ with cross-sections below 0.07×10^{-16} cm^2 (data not shown) and their cross-sections are not analyzed any further. Small amounts of MoS_2^+ are formed by sequential collisions with CS_2, which also lead to the small exothermic feature in the MoS^+ cross-section.

$$Mo^+ + CS_2 \rightarrow MoS^+ + CS \quad (17)$$

$$Mo^+ + CS_2 \rightarrow MoCS^+ + S \quad (18)$$

MoS^+ and $MoCS^+$ are formed according to reactions (17) and (18) and their cross-sections rise from apparent thresholds of 0.3 and 2.3 eV, respectively (Fig. 3). The MoS^+ cross-section has a steep onset and exhibits the highest cross-section ($\sigma_{0,max} =$

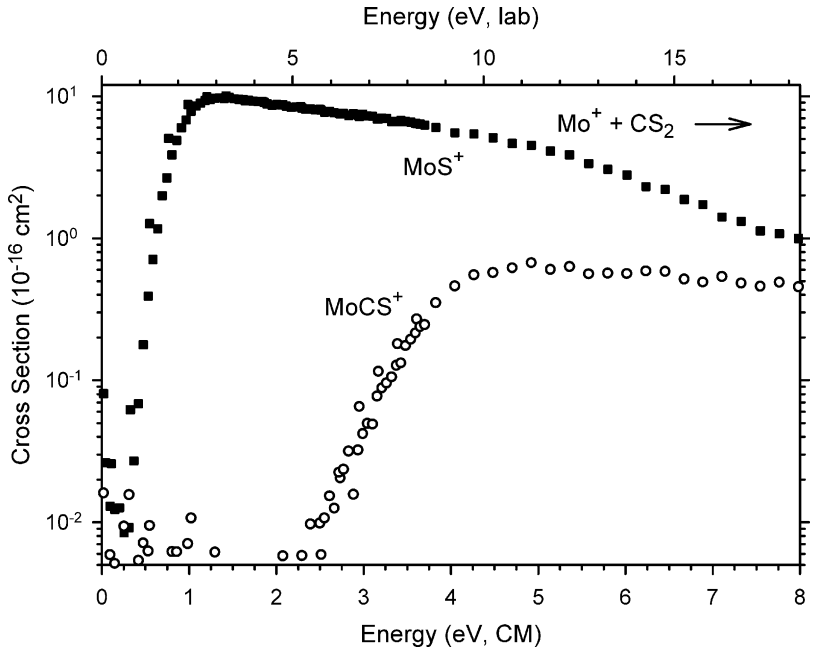

Fig. 3. Product cross-sections for the reactions of Mo^+ with CS_2 to form MoS^+ (■) and $MoCS^+$ (○) as a function of center-of-mass energy (lower axis) and laboratory energy (upper axis).

10×10^{-16} cm^2) of all endothermic reactions with CS_2 studied so far [36]. The MoS^+ cross-section peaks near 1.3 eV and declines smoothly at higher energies. In contrast to the related V^+/CS_2 system [28,29], the MoS^+ cross-section does not show any evidence of a composite behavior. Analysis of the cross-sections with Eq. (1), Table 3, gives thresholds that lead to $D_0(Mo^+–S) = 3.68 \pm 0.06$ eV and $D_0(Mo^+–CS) = 1.68 \pm 0.14$ eV. The former fits well with the crude bracket 3.21 eV $< D_0(Mo^+–S) <$ 4.43 eV

Table 3
Summary of parameters in Eq. (1) used for the fits of the cross-sections for the reactions of CS_2 and Xe with Mo^+, MoS^+, and MoS^+, respectively, reactions (17)–(25)

Reactants	Products	E_0 (eV)[a]	σ_0	n
$Mo^+ + CS_2$	$MoS^+ + CS$	0.82 (0.04)	17.44 (1.11)	0.5 (0.1)
	$MoCS^+ + S$	2.82 (0.13)	1.63 (1.04)	1.7 (0.3)
$MoS^+ + CS_2$[b]	$MoS_2^+ + CS$	0.31 (0.09)	17.25 (1.11)	1.7 (0.2)
	$MoCS_2^+ + S$	3.03 (0.19)	0.29 (0.02)	0.4 (0.2)
	$Mo^+ + [CS_3]$	3.78 (0.15)	3.94 (1.07)	1.6 (0.2)
$MoS_2^+ + Xe$	$MoS^+ + S$	4.12 (0.21)	1.20 (0.54)	2.3 (0.3)
	$Mo^+ + S_2$	3.34 (0.10)	2.49 (0.51)	1.8 (0.2)
$MoS_2^+ + CS_2$	$MoS_3^+ + CS$	1.13 (0.08)	0.72 (0.06)	1.9 (0.2)
	$MoCS_2^+ + S_2$	2.68 (0.13)	0.36 (0.05)	1.3 (0.4)
	$MoS^+ + [CS_3]$	3.90 (0.10)	3.00 (0.53)	2.0 (0.1)
	$Mo^+ + [CS_4]$	3.42 (0.16)	1.46 (0.09)	1.8 (0.1)

[a] The E_0 values are the average of several threshold fits with uncertainties of one standard deviation.
[b] The $MoCS^+$ and CS_2^+ cross-sections are too low and noise for analysis.

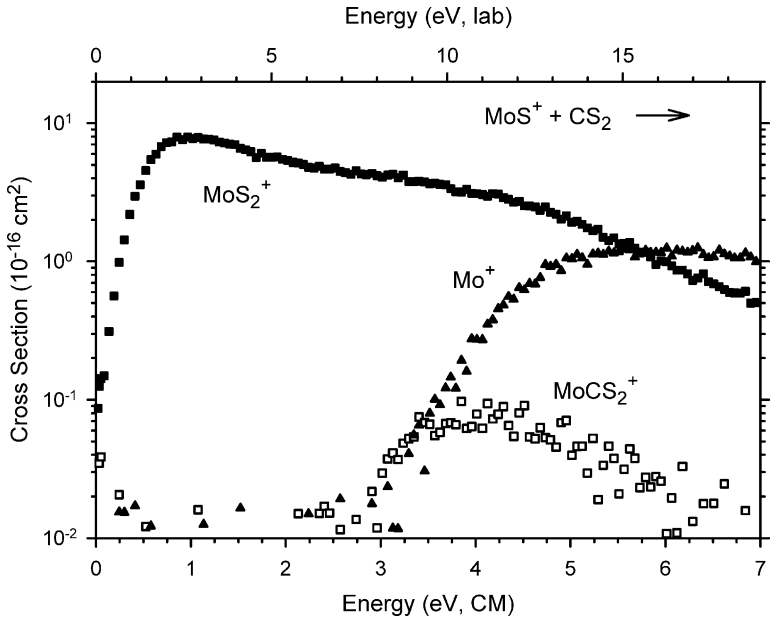

Fig. 4. Product cross-sections for the reactions of MoS^+ with CS_2 to form MoS_2^+ (■), $MoCS_2^+$ (□), and Mo^+ (▲) as a function of center-of-mass energy (lower axis) and laboratory energy (upper axis).

obtained from FTICR bracketing experiments and a CASPT2Drel value of $D_0(Mo^+–S) = 3.45\,eV$ [31].

The leading process in the MoS^+/CS_2 system corresponds to MoS_2^+ formation according to reaction (19). On the basis of the energy behavior, reaction (19) is only slightly endothermic (Fig. 4).

$$MoS^+ + CS_2 \rightarrow MoS_2^+ + CS \quad (19)$$

$$MoS^+ + CS_2 \rightarrow MoCS_2^+ + S \quad (20)$$

$$MoS^+ + CS_2 \rightarrow Mo^+ + [CS_3] \quad (21)$$

Thus, even at the lowest collision energy, reaction (19) bears a finite cross-section. This observation is consistent with the thermal rate constant of $3.3 \times 10^{-11}\,cm^3\,s^{-1}\,molecule^{-1}$ for reaction (19) determined in FTICR measurements [31]. Given a collision rate constant of $1 \times 10^{-9}\,cm^3\,molecule^{-1}\,s^{-1}$, the reaction efficiency is about 3.3%. At elevated energies, $MoCS_2^+$ and Mo^+ are observed as additional products (reactions 20 and 21). Small amounts of CS_2^+ and $MoCS^+$ with $\sigma_{max} < 0.14 \times 10^{-16}\,cm^2$ observed at higher energies are not pursued any further. Analysis of the threshold behavior of reactions (19) and (20) yields $D_0(SMo^+–S) = 4.19 \pm 0.10\,eV$ and $D_0(Mo^+–CS_2) = 0.65 \pm 0.20\,eV$, respectively. The former value agrees with an earlier bracket of $3.73\,eV < D_0(SMo^+–S) < 4.95\,eV$ and a value of 3.76 eV calculated at the CASPT2Drel level of theory [31]. This bond energy can be combined with $D_0(Mo^+–S) = 3.68 \pm 0.06\,eV$ and $D_0(S–S) = 4.364 \pm 0.005\,eV$ to give $D_0(Mo^+–S_2) = 3.51 \pm 0.12\,eV$. This agrees well with a value of $3.47 \pm 0.17\,eV$ obtained from the threshold for reaction (21) given that the neutral products are $CS + S_2$, as also suggested for the analogous process in the vanadium system.

Like for the vanadium analog, the purity of the MoS_2^+ beam can be probed by collision experiments. CID of MoS_2^+ with xenon yields Mo^+ and MoS^+ as products (data not shown) and no oxygen-containing fragments, e.g., MoO^+ and $MoSO^+$, are observed, thereby excluding interference by MoO_2S^+. Formation of Mo^+ has the lower threshold and reaches a cross-section of about $1.6\,Å^2$ near 5.5 eV, at which

point it declines rapidly as a consequence of competition with MoS^+ formation. The cross-section for the MoS^+ product ion reaches a maximum magnitude of about 3.5 Å^2 above 12 eV. Note that the relative magnitudes of these two products differ appreciably from the VS_2^+ system, where the analogous product ions had comparable cross-sections. As found for the vanadium system, competition with the MoS^+ channel affects the shape of the Mo^+ cross-section, such that the threshold for this dissociation reaction is obtained from an analysis of the total cross-section. Analysis of the cross-sections with Eq. (1) yields $E_0(Mo^+) = 3.34 \pm 0.10$ eV and $E_0(MoS^+) = 4.12 \pm 0.21$ eV which can be compared with bond energy values of 3.51 ± 0.12 eV and 4.19 ± 0.10 eV, respectively, as derived from analysis of reaction (19). Thus, just like for VS_2^+, the CID thresholds of mass-selected MoS_2^+ are similar to the bond dissociation energies derived from reaction of MS^+ with CS_2.

The interaction of MoS_2^+ with CS_2 results in formation of MoS_3^+, $MoCS_2^+$, MoS^+, and Mo^+ according to reactions (22)–(25). The cross-sections are depicted in Fig. 5.

$$MoS_2^+ + CS_2 \rightarrow MoS_3^+ + CS \quad (22)$$

$$MoS_2^+ + CS_2 \rightarrow MoCS_2^+ + S_2 \quad (23)$$

$$MoS_2^+ + CS_2 \rightarrow MoS^+ + [CS_3] \quad (24)$$

$$MoS_2^+ + CS_2 \rightarrow Mo^+ + [CS_4] \quad (25)$$

Analysis of the data with Eq. (1) provides $D_0(S_2Mo^+–S) = 3.37 \pm 0.09$ eV and $D_0(Mo^+–CS_2) = 0.74 \pm 0.17$ eV, respectively. This agrees nicely with a lower limit of $D_0(S_2Mo^+–S) > D_0(OC–S) = 3.140 \pm 0.005$ eV derived from the occurrence of sulfur transfer from COS to MoS_2^+ [31]. The value for $D_0(Mo^+–CS_2)$ of 0.74 ± 0.17 eV from reaction (23) also agrees nicely with $D_0(Mo^+–CS_2) = 0.65 \pm 0.20$ eV derived from the threshold of reaction (20) resulting in an average of $D_0(Mo^+–CS_2) = 0.70 \pm 0.13$ eV. As far as reactions (24) and (25) are concerned, comparison of the various thresholds suggests that $CS + S_2$ are most likely formed as the neutral products in reaction (24), whereas the threshold

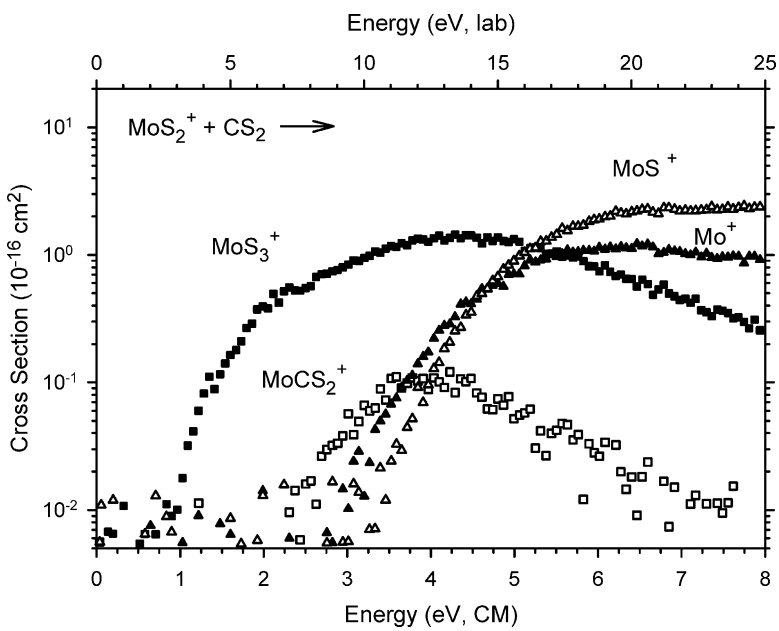

Fig. 5. Product cross-sections for the reactions of MoS_2^+ with CS_2 to form MoS_3^+ (■), $MoCS_2^+$ (□), MoS^+ (△), and Mo^+ (▲) as a function of center-of-mass energy (lower axis) and laboratory energy (upper axis).

of Mo^+ according to reaction (25) is consistent with simple CID of MoS_2^+.

If the threshold results from the six reactions involving MoS_2^+, processes (19), (21), (24), (25), and the two CID reactions are combined as described above for the analogous vanadium systems, average values for $D_0(SMo^+–S)$ and $D_0(Mo^+–S_2)$ can be derived as 4.10 ± 0.10 eV and 3.42 ± 0.11 eV, respectively. These are weighted averages of all six results with an uncertainty of two standard deviations of the mean. The threshold for reaction (24) assumes that $CS + S_2$ neutral products are formed, as this gives the most consistent thermochemistry. Combining $D_0(S_2Mo^+–S) = 3.37 \pm 0.09$ eV with $D_0(SMo^+–S) = 4.10 \pm 0.10$ eV and $D_0(S–S) = 4.364 \pm 0.005$ eV yields $D_0(SMo^+–S_2) = 3.11 \pm 0.13$ eV (Table 1).

4. Theoretical results

In order to gain information about the different structures and electronic states of MS_2^+ species (M = V, Fe, Mo; $n = 2, 3$), quantum-chemical calculations were performed using the hybrid density functional B3LYP. In these calculations, several arrangements of the sulfur atoms were examined. Thus, an MS_2^+ species may bear an *end-on* or *side-on* coordinated S_2 ligand, both denoted as $M(S_2)^+$, or exist as an inserted metal disulfide, termed as SMS^+. Likewise, even more structures can be conceived for MS_3^+ cations. Because some theoretical results of the iron and molybdenum sulfides have been reported before [13,31,37,38], only those structures are described that have not been discussed before.

4.1. Metal disulfide cations

Two isomers, an inserted SVS^+ and a *side-on* $V(S_2)^+$ species, are located in the $[VS_2]^+$ system (Scheme 2). Generally, the S–S bond length for hydrogen persulfide of 2.055 Å [39] is used to differentiate between an S–S bond and two individual sulfur ligands. The global minimum is the disulfur complex in a triplet state, $V(S_2)^+$ ($^3A^1$). The counterparts on the quintet and singlet potential-energy surfaces, $V(S_2)^+$

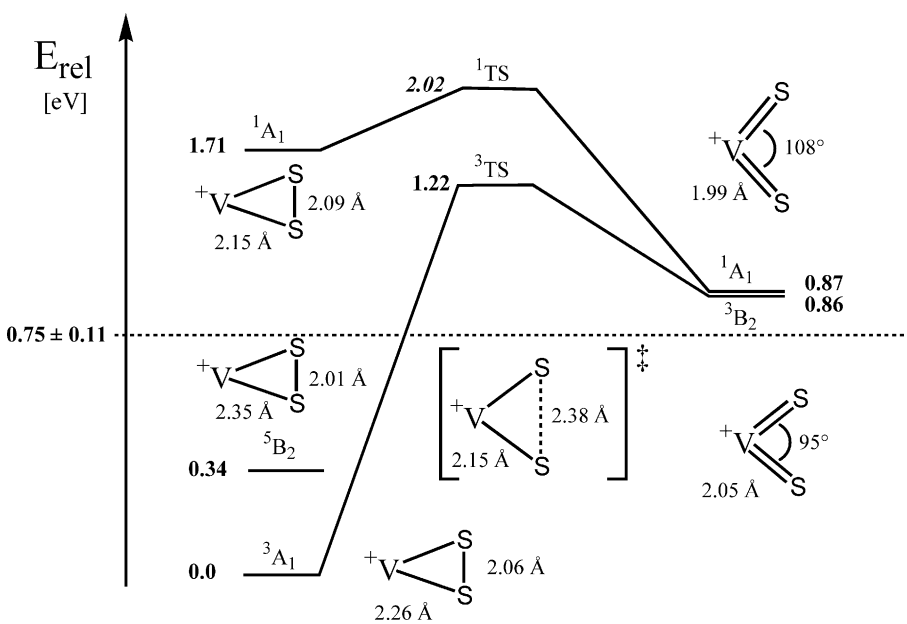

Scheme 2.

($^5B_2$) and $V(S_2)^+$ ($^1A_1$), lie 0.34 and 1.71 eV above $V(S_2)^+$ ($^3A^1$). As far as the inserted species are concerned, the triplet and singlet disulfides, SVS^+ ($^3B_2$) and SVS^+ ($^1A_1$), respectively, are found 0.86 and 0.87 eV higher in energy than $V(S_2)^+$ ($^3A^1$). Note that the energetic proximity of these states does not allow the assignment of either multiplicity to the lowest inserted state. All attempts to locate an inserted quintet structure failed and converged to the *side-on* isomer. Two linear isomers, SVS^+ ($^1\Sigma_g$, $r_{V-S} = 2.07$ Å) and VSS^+ ($^1\Sigma$, $r_{V-S} = 2.04$ Å, $r_{S-S} = 1.91$ Å), are located on the singlet surface ca. 3.6 and 3.5 eV above $V(S_2)^+$ ($^3A^1$). They are therefore considered as high-energy isomers and not pursued any further. Finally, the interconversion of $V(S_2)^+$ and SVS^+ is associated with significant activation barriers. The resulting potential-energy surface (PES) is shown in Scheme 2.

The PES for the $[FeS_2]^+$ system has been described elsewhere [13]. In brief, a *side-on* isomer with a $^6A_1$ ground state has been located as the global minimum, whereas the inserted structure is 1.5 eV higher in energy and also exhibits a $^6A_1$ ground state.

In contrast to vanadium and iron, the insertion species $SMoS^+$ ($^2A_1$) is the most stable species in the $[MoS_2]^+$ system (Scheme 3). This result agrees well with a CASPT2Drel calculation, which also predicted an inserted $^2A_1$ ground state [31]. The corresponding quartet insertion species $SMoS^+$ ($^4A_2$) is 0.81 eV higher in energy than $SMoS^+$ ($^2A_1$) in reasonable agreement with the splitting of 1.13 eV calculated at the CASPT2Drel level of theory. The lowest-lying *side-on* coordinated $Mo(S_2)^+$ ($^4B_1$) is 0.53 eV above $SMoS^+$ ($^2A_1$) with the sextet analog $Mo(S_2)^+$ ($^6B_1$) another 0.31 eV higher in energy. The corresponding doublet $Mo(S_2)^+$ ($^2B_1$) lies 1.47 eV above $SMoS^+$ ($^2A_1$). Despite numerous attempts, no transition structure connecting the inserted and the *side-on* coordinated species could be located. In order to obtain an estimate for the barrier height between the inserted and *side-on* coordinated isomers, linear synchronous transit [40] calculations were performed as well. However, no continuous path could be located because of abrupt changes in the energy and symmetry of the wave function from that of the starting isomer to that of the other isomer. This behavior is indicated by the solid lines in Scheme 3.

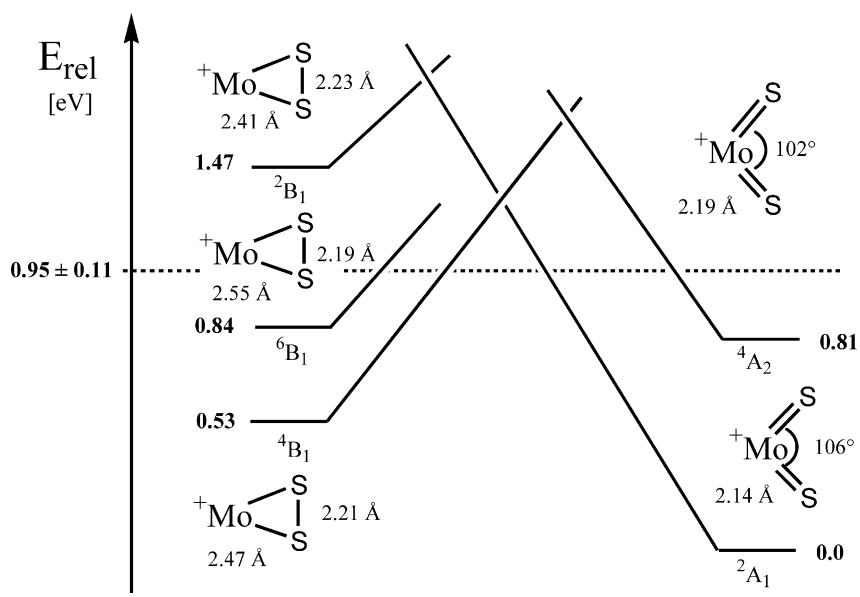

Scheme 3.

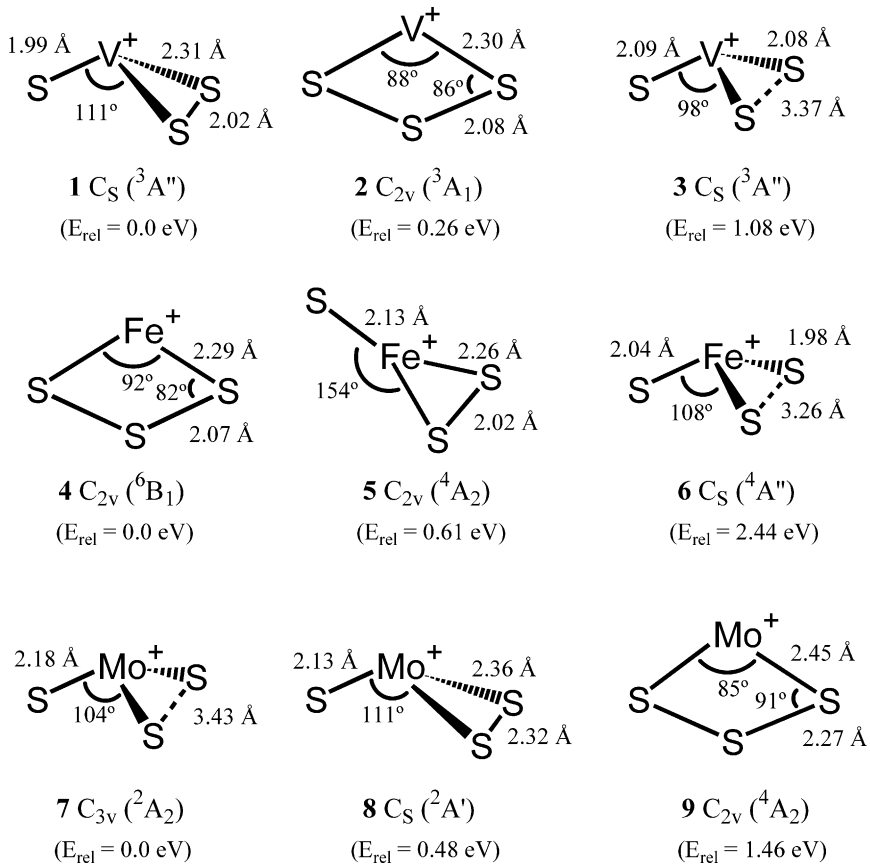

1 C_S (^{3}A") (E_{rel} = 0.0 eV)

2 C_{2v} ($^3A_1$) (E_{rel} = 0.26 eV)

3 C_S (^{3}A") (E_{rel} = 1.08 eV)

4 C_{2v} ($^6B_1$) (E_{rel} = 0.0 eV)

5 C_{2v} ($^4A_2$) (E_{rel} = 0.61 eV)

6 C_S (^{4}A") (E_{rel} = 2.44 eV)

7 C_{3v} ($^2A_2$) (E_{rel} = 0.0 eV)

8 C_S (^{2}A') (E_{rel} = 0.48 eV)

9 C_{2v} ($^4A_2$) (E_{rel} = 1.46 eV)

Scheme 4.

4.2. Metal trisulfide cations

B3LYP calculations of the MS_3^+ systems yield the optimized geometries summarized in Scheme 4. C_S symmetric structures have their reflection plane in the plane of the page. Structure **1** ($^3A''$) is identified as the lowest minimum on the PES of the $[VS_3]^+$ system. Vertical excitations of **1** to the singlet and quintet surfaces yield excitation energies of 0.7 and 1.7 eV, respectively. Further, a planar structure **2** ($^3A^1$) with a bidentate S_3 ligand is located 0.26 eV above **1**. For an almost C_{3v}-symmetrical trisulfide structure **3** ($^3A''$), which lies 1.08 eV above **1**, frequency calculations yield one imaginary mode of *i*66 cm^{-1}, thus identifying **3** as a saddle point.

For iron, the planar structure **4** ($^6B_1$) with an η^2-coordinated S_3 ligand is located as the lowest minimum. Vertical excitation to the doublet and quartet surfaces results in splittings of 0.98 and 0.04 eV, respectively. Geometry optimization of the latter yields a $^4B_1$ state only 0.003 eV above **4** ($^6B_1$) with an almost identical geometry. A planar structure **5** ($^4A_2$) with one intact S_2 ligand is 0.61 eV higher in energy than **4** ($^6B_1$) with a close-lying $^4A_1$ state at 0.73 eV. A C_s-symmetrical iron-trisulfide structure **6** ($^4A''$) is located 2.44 eV above **4**.

In contrast to VS_3^+ and FeS_3^+, MoS_3^+ exhibits a C_{3v}-symmetrical ground state **7** ($^2A_2$) with a metal trisulfide structure. This result is in good agreement with the results of previously published calculations

at the B3LYP level of theory [31]. Vertical excitation to the quartet and sextet surfaces requires 0.94 and 2.7 eV, respectively. Attempts to locate structures with intact S_2 ligands led to the C_s-symmetrical minimum **8** ($^2A'$), which is 0.48 eV more energetic than **7** ($^2A_2$). In analogy to **2** and **4**, structure **9** ($^4A_2$) with an intact S_3 ligand is located 1.46 eV above **7** ($^2A_2$). A similar, although non-planar polysulfide structure is found at a much lower energy (0.65 eV), when larger basis sets are used for Mo and S [31]. The geometry of **9** and that reported in [31] differ in that **9** has slightly longer Mo–S and S–S bonds ($r_{Mo–S} = 2.45$ Å vs. 2.34 Å and $r_{S–S} = 2.27$ Å vs. 2.11 Å). These findings point to the insufficiency of the 3-21G basis sets used for Mo and S in the present study.

The structural differences observed for the metal trisulfides can be understood as a result of the accessible oxidation states of the three metals. Thus, vanadium and molybdenum can adopt the maximal oxidation states +5 and +6, respectively, whereas iron prefers the lower oxidation states +2 and +3. Accordingly, the most stable species can be predicted from consideration of the number of valence electrons in the respective MS_3^+ systems. Thus, VS_3^+ has at least one intact S_2 ligand, the MoS_3^+ species can exist as a genuine trisulfide, and FeS_3^+ is predicted to bear a coordinated S_3 ligand.

5. Discussion

The experimental findings in conjunction with the calculated potential-energy surfaces indicate that sequential sulfur-atom transfer from COS to V^+ and Mo^+ could lead to a mixture of $M(S_2)^+$ and SMS^+ isomers. Quite interestingly, the ab initio calculations predict $V(S_2)^+$ to be more stable than SVS^+, whereas $SMoS^+$ is preferred over $Mo(S_2)^+$. By combining the experimental and theoretical results, the formation and interconversion of these isomers under flow tube conditions can be understood in more detail.

In the case of vanadium, $D_0(SV^+–S) = 3.89 \pm 0.11$ eV derived above, implies $\Delta_R H(14) = -0.75 \pm 0.11$ eV (indicated by the dashed line in Scheme 2). Given the computed energy difference of ca. 0.86 eV between ground-state $V(S_2)^+$ and SVS^+, sulfur transfer from COS to VS^+ ($^3\Sigma^-$) is therefore unlikely to allow formation of SVS^+ at thermal energies. Although participation of small amounts of the SVS^+ isomer cannot be ruled out, there is no decisive experimental evidence for two isomers in the mass-selected $[VS_2]^+$ beam either in reaction with CS_2 or CID with Xe. However, the possibility of forming two different isomers for VS_2^+ may be the origin of the complicated behavior in the cross-section observed for the VS_2^+ product channel of reaction (3) at intermediate energies, as described above. Here, reaction (3) is postulated to form ground-state $V(S_2)^+$ at low energies, but beginning at about 1.4 eV (the sum of the threshold measured for reaction (3) and the excitation energy for the SVS^+ isomer), an alternate pathway for formation of VS_2^+ opens.

Likewise, sequential sulfur-atom transfer from COS to Mo^+ is associated with considerable exothermicities. In particular, the thermochemistry derived above implies that the sulfur-atom transfer from COS to MoS^+ is 0.95 ± 0.11 eV exothermic (dashed line in Scheme 3). In this case, the reaction may therefore not only yield the more stable $SMoS^+$ disulfide, but also allow for formation of the more energetic $Mo(S_2)^+$ species. The barriers between the inserted and *side-on* isomers may prevent interconversion of $Mo(S_2)^+$ and $SMoS^+$, thereby allowing for the formation of a mixture of both isomers in gas phase experiments. However, no experimental evidence for the excited state isomer is observed in these experiments.

The possibility of different isomers for MS_2^+ (M = V and Mo) in the ion beam becomes especially interesting for the interpretation of the Xe CID and CS_2 reaction data and the observed differences for the two metals. For CID of VS_2^+, the cross-sections for V^+ and VS^+ have comparable intensities, whereas CID of MoS_2^+ yields a MoS^+ cross-section that greatly exceeds the Mo^+ cross-section. These observations can be rationalized by the differing ground-state geometries in the two systems. VS_2^+ exists in a $V(S_2)^+$ ground state with an intact S_2 ligand. Collisional activation with Xe disrupts the $V^+–S_2$ bond and leads to

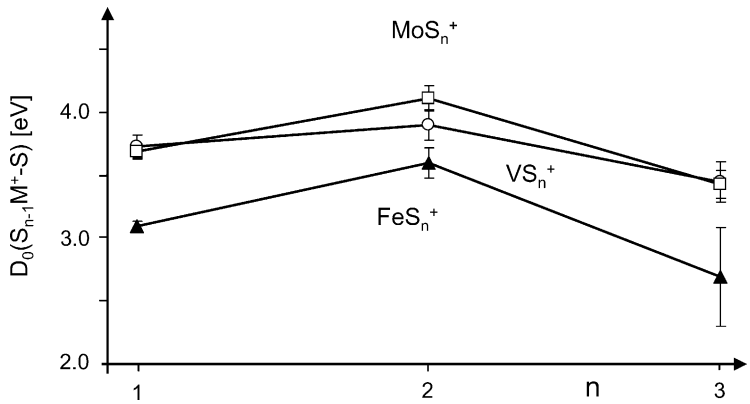

Fig. 6. Variation of the experimental $S_{n-1}M^+$–S bond strengths in MS_n^+ cations (M = V, Fe, and Mo; n = 1–3).

efficient formation of V^+. At higher collision energies, part of the energy deposited in the collision can be used for isomerization into the inserted SVS^+ species, which can then lose a single S ligand resulting in a VS^+ product cross-section of comparable magnitude. In contrast, MoS_2^+ has an inserted $SMoS^+$ ground state such that S_2 ligand loss to yield Mo^+ requires rearrangement, thereby making it unfavorable as indicated by the much smaller cross-section magnitude. At higher energies, the kinetically more favorable MoS^+ formation from $SMoS^+$ can begin and supercedes Mo^+ formation within 2 eV. In reaction with CS_2, the ligand displacement reactions (10) and (20) can be compared (Figs. 2 and 5). Note that this cross-section is much larger in the vanadium system, consistent with facile replacement of the S_2 ligand from $V(S_2)^+$, whereas in the molybdenum system, the process is less likely, presumably because it would again involve a more complex rearrangement to eliminate S_2.

With the results presented above, we can attempt a comparison of the thermochemical properties of the transition-metal mono-, di-, and trisulfide cations of vanadium, iron and molybdenum. Synergistic effects are of major interest, i.e., the influence of one ligand on the bond strength of another. The comparison of the vanadium and the iron triad may highlight the differences and similarities of early vs. late metal sulfides of the first transition row. Likewise, consideration of the vanadium and molybdenum triads may allow some insight into the effects caused by substitution of a first-row by a second-row transition-metal [9] (Fig. 6).

As far as synergistic effects are considered, all three metal sulfides exhibit a maximum in bond strength for the second sulfur ligand. The maximum at MoS_2^+ in the molybdenum triad has previously been attributed to reduced bond energies of MoS^+ and MoS_3^+ [31]. The reduction of the former is caused by the occupation of slightly anti-bonding orbitals and the favorable half-shell d^5 configuration of the Mo^+ fragment, whereas the latter results from a deficiency of unpaired valence electrons on the Mo-center for formation of strong bonds between the doublet MoS_2^+ ground state and the third sulfur. The increase in bond strength going from $D_0(M^+–S)$ to $D_0(SM^+–S)$ with M = V and Fe can be rationalized by the finding that VS_2^+ and FeS_2^+ exhibit cyclic, *side-on* structures as ground states. Thus, $D_0(SM^+–S)$ should more correctly be termed as the reaction enthalpy $M(S_2)^+ \rightarrow MS^+ + S$ for M = V and Fe. The lower bond energies for the third sulfur ligand in the $[VS_3]^+$ system can be rationalized by the higher formal oxidation state of the metal center. For FeS_3^+ the decrease of the M–S bond strength from $D_0(SFe^+–S)$ to $D_0(S_2Fe^+–S)$ is consistent with the presence of an intact S_3 ligand (Scheme 4) in that $D_0(S–S) = 4.364\,eV > D_0(S_2–S) = 2.71\,eV$ (Table 1). Nevertheless, the formation of FeS_3^+ in the reaction of FeS_2^+ with COS under thermal conditions sheds some doubt upon the

$D_0(S_2Fe^+–S) = 2.68 \pm 0.39$ eV value derived from the PD threshold of the $[FeS_3]^+$ cation [30]. Possibly, isomeric mixtures were probed in the PD measurement or the ions were not completely thermalized. Further, considering the bond strengths of the metal–S_2 interaction in the di- and trisulfides, it emerges that the addition of sulfur atoms to the metal cations reduces the abilities of the metal centers to bind S_2 ligands, i.e., $D_0(M^+–S_2) < D_0(SM^+–S_2)$ for M = V, Mo, and Fe. This finding may serve as an explanation for the general observation that MS_n^+ species with $n > 3$ prefer the loss of an S_2 unit over the loss of a single S atom upon collisional activation [41].

6. Conclusions

The bond dissociation energies for losses of S and S_2 from the di- and trisulfide compounds of vanadium and molybdenum have been derived. Calculations at the B3LYP level of theory predict *side-on* geometries for the ground states of VS_2^+ and FeS_2^+, whereas molybdenum, as a metal of the second transition row, exhibits an inserted $SMoS^+$ structure. This difference can be related to the larger spatial extent of the 4d orbitals as well as the preference of high oxidation states for molybdenum. For the MS_3^+ cations, theory predicts structures with intact S_2 and S_3 units for VS_3^+ and FeS_3^+, respectively, and a trisulfide structure with three single S ligands for MoS_3^+.

The following binding energies (all in eV) are derived: $D_0(SV^+–S) = 3.89 \pm 0.11$, $D_0(V^+–S_2) = 3.25 \pm 0.14$, $D_0(S_2V^+–S) = 3.44 \pm 0.16$, $D_0(SV^+–S_2) = 2.97 \pm 0.19$, $D_0(V^+–CS_2) = 1.18 \pm 0.13$, $D_0(Mo^+–S) = 3.68 \pm 0.06$, $D_0(SMo^+–S) = 4.10 \pm 0.10$, $D_0(Mo^+–S_2) = 3.42 \pm 0.11$, $D_0(S_2Mo^+–S) = 3.37 \pm 0.09$, $D_0(SMo^+–S_2) = 3.11 \pm 0.13$, $D_0(Mo^+–CS) = 1.68 \pm 0.14$, and $D_0(Mo^+–CS_2) = 0.70 \pm 0.13$.

Acknowledgements

This work was supported by the Deutsche Forschungsgemeinschaft, the Fonds der Chemischen Industrie, and the Freunde der Technischen Universität Berlin, and the National Science Foundation (PBA, CHE-0135517). In addition, we thank the Konrad-Zuse Institut, Berlin, for the generous allocation of computer time.

References

[1] R.L. Rawls, Chem. Eng. News 79 (2001) 48.
[2] E.I. Stiefel, K. Matsumoto (Eds.), Transition Metal Sulfur Chemistry, ACS Symposium Series 653, Am. Chem. Soc., Washington, DC, 1996.
[3] W. Kaim, B. Schwederski, Bioanorganische Chemie, Teubner, Stuttgart, 1991.
[4] (a) H. Beinert, R.H. Sands, Biochim. Biophys. Res. Commun. 3 (1960) 41;
(b) R.H. Sands, H. Beinert, Biochim. Biophys. Res. Commun. 3 (1960) 47.
[5] H. Beinert, JBIC 5 (2000) 2.
[6] A. Müller, E. Krahn, Angew. Chem. Int. Ed. Engl. 34 (1995) 1071.
[7] D. Sellmann, J. Sutter, Acc. Chem. Res. 30 (1997) 460.
[8] F. Tuczek, N. Lehnert, Angew. Chem. Int. Ed. Engl. 37 (1998) 2636.
[9] W. Kaim, B. Schwederski, Bioanorganische Chemie, 2nd ed., Teubner, Stuttgart, 1995.
[10] O. Einsle, F.A. Tezcan, S.L.A. Andrade, B. Schmid, M. Yoshida, J.B. Howard, D.C. Rees, Science 297 (2002) 1696.
[11] I.V. Kurnikov, A.K. Charnley, D.N. Beratan, J. Phys. Chem. B 105 (2001) 5359.
[12] K. Koszinowski, D. Schröder, H. Schwarz, R. Liyanage, P.B. Armentrout, J. Chem. Phys. 117 (2002) 10039.
[13] D. Schröder, I. Kretzschmar, H. Schwarz, C. Rue, P.B. Armentrout, Inorg. Chem. 38 (1999) 3474.
[14] K.M. Ervin, P.B. Armentrout, J. Chem. Phys. 83 (1985) 166.
[15] R.H. Schultz, P.B. Armentrout, Int. J. Mass Spectrom. Ion Process. 107 (1991) 29.
[16] F.A. Khan, D.L. Steele, P.B. Armentrout, J. Phys. Chem. 99 (1995) 7819 (and references therein).
[17] D.E. Clemmer, Y.-M. Chen, F.A. Khan, P.B. Armentrout, J. Phys. Chem. 98 (1994) 6522.
[18] C.L. Haynes, P.B. Armentrout, Organometallics 13 (1994) 3480.
[19] D. Gerlich, in: C.Y. Ng, M. Baer (Eds.), State-Selected and State-to-State Ion–Molecule Reaction Dynamics. Part 1. Experiment. Advances in Chemical Physics Series, vol. LXXXII, Wiley, New York, 1992, p. 1.
[20] K. Eller, H. Schwarz, Int. J. Mass Spectrom. Ion Process. 93 (1989) 243.
[21] K. Eller, W. Zummack, H. Schwarz, J. Am. Chem. Soc. 112 (1990) 621.
[22] U. Mazurek, H. Schwarz, ICR Kinetics, version 3.0.1, TU Berlin, 1998.

[23] D. Schröder, H. Schwarz, D.E. Clemmer, Y.-M. Chen, P.B. Armentrout, V.I. Baranov, D.K. Böhme, Int. J. Mass Spectrom. Ion Process. 161 (1997) 177.
[24] P.J. Stevens, F.J. Devlin, C.F. Chablowski, M.J. Frisch, J. Phys. Chem. 98 (1994) 11623.
[25] M.J. Frisch, G.W. Trucks, H.B. Schlegel, P.M.W. Gill, B.G. Johnson, M.A. Robb, J.R. Cheeseman, T. Keith, G.A. Petersson, J.A. Montgomery, K. Ragavachari, M.A. Al-Laham, V.G. Zakrezewski, J.V. Oritz, J.B. Foresman, C.Y. Peng, P.Y. Ayala, W. Chen, M.W. Wong, J.L. Andres, E.S. Replogle, R. Gomperts, R.L. Martin, D.J. Fox, J.S. Binkley, X. DeFrees, J. Baker, J.J.P. Stewart, M. Head-Gordon, C. Gonzales, J.A. Pople, Gaussian Inc., Pittsburgh, PA, 1995.
[26] M. Brönstrup, D. Schröder, I. Kretzschmar, H. Schwarz, J. Am. Chem. Soc. 123 (2001) 142.
[27] K. Raghavachari, G.W. Trucks, J. Chem. Phys. 91 (1989) 1062.
[28] I. Kretzschmar, D. Schröder, H. Schwarz, C. Rue, P.B. Armentrout, J. Phys. Chem. A 102 (1998) 10060.
[29] C. Rue, P.B. Armentrout, I. Kretzschmar, D. Schröder, J.N. Harvey, H. Schwarz, J. Chem. Phys. 110 (1999) 7858.
[30] T.J. MacMahon, T.C. Jackson, B.S. Freiser, J. Am. Chem. Soc. 111 (1989) 421.
[31] I. Kretzschmar, A. Fiedler, J.N. Harvey, D. Schröder, H. Schwarz, J. Phys. Chem. A 101 (1997) 6252.
[32] D. Sülzle, H. Egsgaard, L. Carlsen, H. Schwarz, J. Am. Chem. Soc. 112 (1990) 3750.
[33] R.D.J. Froese, J.D. Goddard, J. Chem. Phys. 96 (1992) 7449.
[34] R.H. Schultz, K.C. Crellin, P.B. Armentrout, J. Am. Chem. Soc. 113 (1991) 8590.
[35] J.R. Brown, P. Schwerdtfeger, D. Schröder, H. Schwarz, J. Am. Soc. Mass Spectrom. 13 (2002) 485.
[36] I. Kretzschmar, D. Schröder, H. Schwarz, P.B. Armentrout, in: M.A. Duncan (Ed.), Advances in Metal and Semiconductor Clusters: Metal–Ligand Bonding and Metal–Ion Solvation, vol. 5, Elsevier, New York, 2001, p. 347.
[37] O. Hübner, J. Sauer, Chem. Phys. Lett. 294 (1998) 37.
[38] O. Hübner, J. Sauer, J. Chem. Phys. 116 (2000) 617.
[39] D.R. Lide, CRC Handbook of Chemistry and Physics, CRC Press, Boca Raton, 1998/99.
[40] T.A. Halgren, W.N. Lipscomb, Chem. Phys. Lett. 49 (1977) 225.
[41] I. Kretzschmar, PhD Thesis, Technische Universität, Berlin, Energetics and Reactivity of the Binary Transition-Metal Sulfides of the 3rd and 4th Row Shaker Verlag, Aachen, 1999.
[42] M.W. Chase (Ed.), NIST-JANAF Thermochemical Tables, 4th ed., J. Phys. Chem. Ref. Data, Monograph No. 9, American Chemical Society, 1998.
[43] D.A. Prinslow, P.B. Armentrout, J. Chem. Phys. 94 (1991) 3563.
[44] J.B. Pedley, R.D. Naylor, S.P. Kirby, Thermochemical Data of Organic Compounds, Chapman & Hall, London, 1986.
[45] L. Capron, W.Y. Feng, C. Lifshitz, B. Tjelta, P.B. Armentrout, J. Phys. Chem. 100 (1996) 16571.